

Effect of a CeO₂ Promoter on Physicochemical Properties and Activity of a 10%Co/Al₂O₃ Catalyst for CH₄ and CO₂ Reforming

Ngoc Thang Tran*, My Hien Thi Bach, Thanh Nha Thi Tran

Faculty of Chemical Engineering, Industrial University of Ho Chi Minh City, No.12 Nguyen Van Bao, Hanh Thong Ward, Ho Chi Minh City, Viet Nam
tranngocthang@iuh.edu.vn

This study investigates the effect of a CeO₂ promoter on the physicochemical properties and catalytic activity of a mesoporous Al₂O₃-supported cobalt catalyst for the CH₄ reforming reaction with CO₂. The Al₂O₃ carrier was synthesized using Al(NO₃)₃·9H₂O as the salt precursor and Pluronic® P-123 as the pore-directing agent, with 75% C₂H₅OH as the solvent. Cobalt oxide and cerium oxide were deposited onto the Al₂O₃ carrier via the capillary impregnation method. The incorporation of cerium oxide was found to reduce the cobalt oxide particle size and facilitate the catalyst activation process. The yields of CO and H₂ were higher for the 3%Ce-10%Co/Al₂O₃ catalyst compared to the 10%Co/Al₂O₃ catalyst. Furthermore, a H₂/CO ratio close to 1 was identified as optimal for Fischer-Tropsch synthesis. Additionally, carbon residues on the surface of the 3%Ce-10%Co/Al₂O₃ catalyst underwent rapid *in situ* oxidation, facilitating the reaction and maintaining the catalyst's stability.

1. Introduction

The increase in CO₂ emissions from industrial production and oil and gas exploitation activities is a major cause of global warming, leading to complex developments of natural disasters, storms and floods. Reducing CO₂ emissions is the responsibility of all countries worldwide. The 26th Conference of the Parties (COP26) to the United Nations Framework Convention on Climate Change emphasized the objective of restricting the global temperature increase to 1.5 K. Meeting this goal necessitates significant and sustained cuts in CO₂ emissions, including a 45% reduction by 2030 relative to 2010 levels and achieving carbon neutrality by the mid-21st century (Arora and Mishra, 2021). Suggested solutions to reduce CO₂ include: (1) limiting emissions, (2) collecting and storing CO₂, and (3) converting CO₂ into production materials. Among these, the last option is the most feasible and promising (Jiang et al., 2020). Carbon in CO₂ is the main component of many important materials such as hydrocarbons, syngas, high molecular compounds... and CH₄ reforming with CO₂ has been considered a potential reaction for converting CO₂ to valuable intermediate, syngas, as represented by Equation (1) (Hernández *et al.*, 2017).



This reaction is endothermic in nature and effective catalysts are noble metals such as Rh, Ru and Pd (Liang *et al.*, 2024). However, their high cost and limited availability present significant barriers to their use in industrial applications (Nguyen *et al.*, 2024). The development of a catalyst system with high activity and stability under reaction conditions is therefore crucial for advancing CH₄ reforming with CO₂ from the research stage to industrial implementation. In contrast, cobalt- and nickel-based catalysts are more affordable and widely available, but they often suffer from lower efficiency and rapid deactivation during reactions (Alhassan *et al.*, 2024). Catalyst support and promoters play a crucial role in catalyst performance for reforming reaction. Our previous research has revealed that γ -Al₂O₃ possessed filament-shaped morphology could effectively disperse Co₃O₄ nanoparticles with small crystallite size. The catalyst exhibited an outstanding performance comparable

to noble metals with the desired ratio of H₂/CO for downstream Fischer-Tropsch process (Tran *et al.*, 2021). Additionally, rare earth metal oxides having basic characteristics could promote CO₂ adsorption and enhance the catalyst activity in CH₄ reforming with CO₂. The synergistic effects of these promoters and distinct γ -Al₂O₃ supports were rarely elucidated. This study investigated a cerium-cobalt catalyst supported by the filament-shaped Al₂O₃, focusing on its performance in CH₄ reforming with CO₂. Additionally, the influence of cerium on the physicochemical properties and catalytic activity was thoroughly examined.

2. Methods

2.1 Catalyst synthesis

The synthesis of the Al₂O₃ support and catalysts utilized the following chemicals: Al(NO₃)₃·9H₂O, Co(NO₃)₂·6H₂O, Ce(NO₃)₃·6H₂O, HCl solution (37%) (Merck), Pluronic® P-123 (Sigma-Aldrich), C₂H₅OH (VWR Chemicals), and double-distilled water. To prepare the Al₂O₃ support, 3.92 g of P123 was dissolved in 59 mL of a 75% (v/v) C₂H₅OH solution with continuous stirring for 30 minutes. Subsequently, 14.72 g of Al(NO₃)₃·9H₂O and 6.28 mL of HCl solution were added, and the mixture was stirred for an additional hour at room temperature. The prepared mixture was transferred to an autoclave and subjected to hydrothermal treatment at 373 K for 24 hours in a drying oven. Following this process, the resulting gel was transferred to an open beaker and dried at 333 K for 48 hours. The dried material was then calcined at 1073 K for 5 hours at a heating rate of 1 K min⁻¹ to yield white Al₂O₃. The final product was ground to a particle size of 125–160 μ m for further use. In our previous reforming studies, the optimal loadings of the promoter and active metal were 3% and 10%, respectively (Tran *et al.*, 2020). Thus, these empirical loadings were applied again in this study for selecting the recipe of promoted catalyst. The catalysts 3%Ce-10%Co/Al₂O₃ and 10%Co/Al₂O₃ were synthesized via the capillary impregnation method. In this approach, Co(NO₃)₂·6H₂O or a combination of Co(NO₃)₂·6H₂O, Ce(NO₃)₃·6H₂O was dissolved in C₂H₅OH to form the precursor solution. This solution was impregnated onto the Al₂O₃ support, followed by stirring for 1 hour. The resulting mixture was dried overnight at 373 K and subsequently calcined at 873 K for 5 hours.

2.2 Catalyst characterization and activity evaluation

The physicochemical properties of the catalysts were characterized using various techniques: (1) N₂ adsorption/desorption was analyzed with a Tristar II 3020 (Micromeritics); (2) X-ray diffraction (XRD) was performed using a Miniflex 600 spectrometer (Rigaku); (3) Temperature-programmed reduction with H₂ (H₂-TPR) was conducted on an AutoChem II-2920 (Micromeritics); (4) HRTEM imaging of the support, fresh catalysts, and spent catalysts was carried out using a TOPCOM EM-002B instrument; and (5) the carbon residue on the catalyst after the reaction was quantified through temperature-programmed oxidation (TPO) analysis on a TGA Q500 (TA Instruments). Catalytic activity was assessed in a tubular reactor with a fixed catalyst bed. The reactor had dimensions of 17 × 3/8 in. (length × diameter). The reaction temperatures for each catalyst were 923 K, 1023 K, and 1073 K. The parameters held constant during each evaluation included a catalyst mass of 0.1 g, a feedstock ratio of 1, and a total gas hourly space velocity (GHSV) of 36 L g_{cat}⁻¹ h⁻¹. The N₂ flow rate was maintained at 60 mL min⁻¹. Prior to the activity assessment, the catalyst was reduced by H₂ to 1023 K for 1 hour, with the reduction gas mixture consisting of 50% H₂ in N₂. The reaction products were analyzed by gas chromatography using a thermal conductivity detector (TCD).

3. Results and discussion

3.1 Catalyst analysis

Figure 1 displays the N₂ adsorption/desorption profiles and pore size distribution for Al₂O₃, 10%Co/Al₂O₃ and 3%Ce-10%Co/Al₂O₃ samples. The adsorption/desorption curves of all three materials are classified as type IV with an H1 hysteresis loop. According to the IUPAC classification, these materials are mesoporous with cylindrical pores (Ali *et al.*, 2024). The hysteresis loop for all three samples appears in a narrow pressure range, indicating large and uniform pore sizes. It is noteworthy that the N₂ adsorption/desorption profiles of the three materials are quite similar, suggesting that the support structure remains largely unchanged after the addition of cobalt oxide and cerium oxide. This indicates that the catalyst particles and promoters are uniformly distributed within the mesoporous structure, without causing any blockage or clogging of the pore openings. The pore size distribution of the materials was calculated using the Barrett–Joyner–Halenda (BJH) method, based on the desorption branch, as shown in Figure 1b. The pore diameters of the materials range from 2 to 11 nm. The average pore size of 3%Ce-10%Co/Al₂O₃ is 5.5 nm, which is smaller compared to that of the Al₂O₃ support and the 10%Co/Al₂O₃ catalyst (6.0 nm). The leftward shift of the pore size distribution curve, observed after simultaneous impregnation of cobalt oxide and cerium oxide onto the Al₂O₃ support, can be attributed to the dilution effect of the cobalt and cerium salt precursors during the

preparation of impregnation solution. The cobalt and cerium ions mix in the solution, resulting in the formation of smaller catalyst and promoter particles, which are incorporated deeper into the mesoporous structure of the support. This phenomenon has also been reported in previous studies (Tran *et al.*, 2020).

The material properties are summarized in Table 1. The specific surface area of the Al_2O_3 support is $173.36 \text{ m}^2 \text{ g}^{-1}$, which decreases to $141.90 \text{ m}^2 \text{ g}^{-1}$ after Co impregnation. However, when both Co and Ce are impregnated simultaneously, the specific surface area of $3\%\text{Ce-}10\%\text{Co}/\text{Al}_2\text{O}_3$ increases by 15% compared to $10\%\text{Co}/\text{Al}_2\text{O}_3$ ($162.96 \text{ m}^2 \text{ g}^{-1}$ vs. $141.90 \text{ m}^2 \text{ g}^{-1}$), while the Co_3O_4 crystal size decreases from 7.75 nm to below 5.0 nm in the presence of cerium salt during impregnation. These findings support the structural analysis based on N_2 adsorption/desorption. The reduction in Co_3O_4 particle size is beneficial for enhancing catalytic activity and minimizing carbon deposition on the catalyst surface.

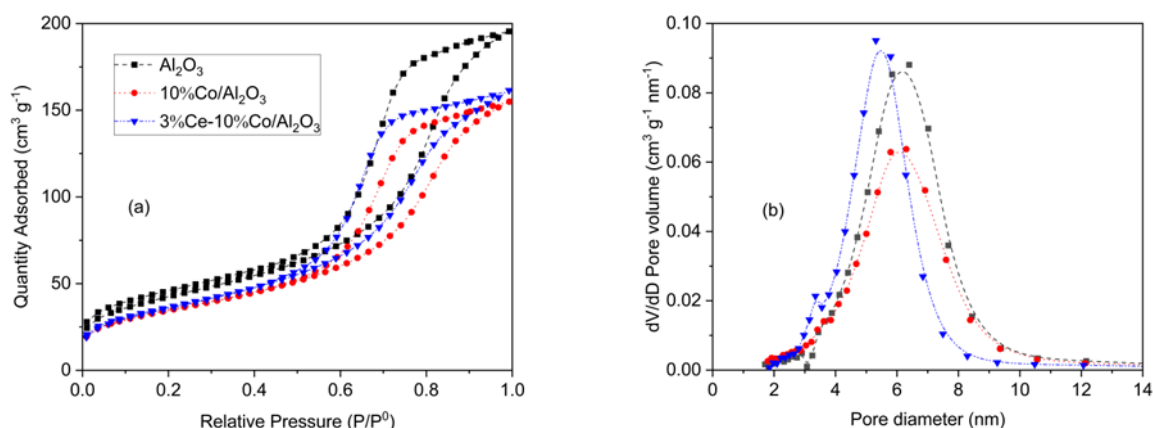


Figure 1: (a) The adsorption/desorption curves and (b) Pore size distribution (b) of Al_2O_3 , $10\%\text{Co}/\text{Al}_2\text{O}_3$, $3\%\text{Ce-}10\%\text{Co}/\text{Al}_2\text{O}_3$

Table 1: Physical properties of Al_2O_3 , $10\%\text{Co}/\text{Al}_2\text{O}_3$, $3\%\text{Ce-}10\%\text{Co}/\text{Al}_2\text{O}_3$

Material	Specific surface area ($\text{m}^2 \text{ g}^{-1}$)	Average pore volume ($\text{cm}^3 \text{ g}^{-1}$)	Average pore diameter (nm)	Co_3O_4 crystal size (nm)
Al_2O_3	173.36	0.28	6.48	-
$10\%\text{Co}/\text{Al}_2\text{O}_3$	141.90	0.22	6.28	7.75
$3\%\text{Ce-}10\%\text{Co}/\text{Al}_2\text{O}_3$	162.96	0.23	5.79	1.89

X-ray diffraction (XRD) analysis offers further insight into the morphology and structure of the materials, with results displayed in Figure 2a. The appearance of peaks at 37.40° , 39.58° , 45.96° , 60.76° , 67.02° , and 77.10° for all three materials confirms that the Al_2O_3 support is in the gamma phase (Khivantsev *et al.*, 2021). The structure of the support remains unchanged during impregnation. The XRD patterns of $10\%\text{Co}/\text{Al}_2\text{O}_3$ and $3\%\text{Ce-}10\%\text{Co}/\text{Al}_2\text{O}_3$ show peaks at 2θ values of 31.32° , 37.03° , 44.88° , and 55.82° , indicative of cobalt oxide in the Co_3O_4 form (JCPDS number 74-2120), while peaks at 59.62° and 65.42° correspond to cobalt aluminate (CoAl_2O_4) (JCPDS number 82-2246). Noticeably, peaks associated with CeO_2 are observed at $2\theta = 28.96^\circ$ and 57.56° with low intensity in the XRD pattern of $3\%\text{Ce-}10\%\text{Co}/\text{Al}_2\text{O}_3$, suggesting that the CeO_2 crystals are small and uniformly dispersed on the support.

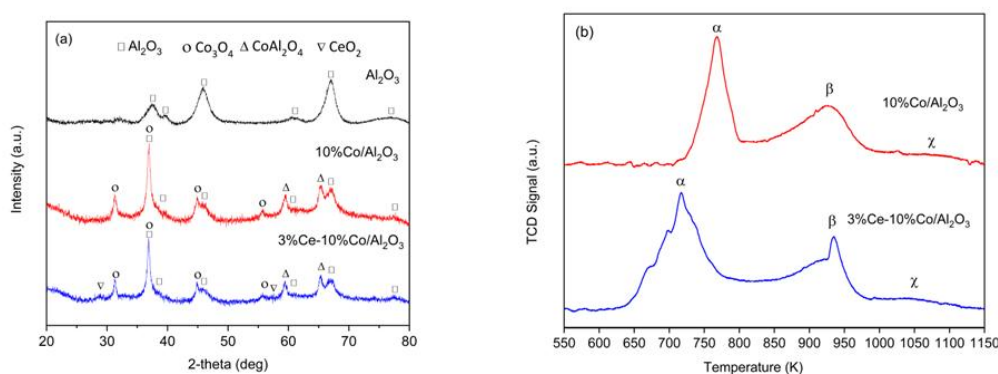


Figure 2: (a) The XRD spectra of Al_2O_3 , $10\%\text{Co}/\text{Al}_2\text{O}_3$, $3\%\text{Ce-}10\%\text{Co}/\text{Al}_2\text{O}_3$ and (b) H_2 -TPR spectra of $10\%\text{Co}/\text{Al}_2\text{O}_3$, $3\%\text{Ce-}10\%\text{Co}/\text{Al}_2\text{O}_3$

The reduction properties of 10%Co/Al₂O₃ and 3%Ce-10%Co/Al₂O₃ were investigated through H₂-TPR analysis, as shown in Figure 2b. The H₂-TPR spectra of both materials display three distinct peaks: one corresponding to the reduction of Co³⁺ (in Co₃O₄) to Co²⁺ (700–770 K), another corresponding to the reduction of Co²⁺ to Co⁰ (930–960 K), and a third corresponding to the reduction of Co²⁺ in CoAl₂O₄ to Co⁰ (above 1000 K). The relatively low intensity of the final peak suggests that the amount of CoAl₂O₄ present in the catalyst is minimal. Typically, cobalt in CoAl₂O₄ is strongly bound to Al₂O₃, resulting in the lack of catalytic activity. It is noteworthy that the reduction of Co³⁺ to Co²⁺ in the 3%Ce-10%Co/Al₂O₃ catalyst takes place at a lower temperature compared to the 10%Co/Al₂O₃ catalyst, suggesting that the catalyst is more readily activated, thereby improving its catalytic activity for the CH₄ reforming reaction with CO₂.

3.2 Catalytic Activity Evaluation

The conversion of CH₄ and CO₂ in the CH₄ reforming reaction with CO₂ over the two catalysts, 10%Co/Al₂O₃ and 3%Ce-10%Co/Al₂O₃, as a function of time, is illustrated in Figures 3(a-d). The conversion of both reactants increases with the reaction temperature, rising from 973 to 1073 K. Specifically, the average CH₄ conversion increases from 47.5% to 76.3%, while the CO₂ conversion increases from 58.2% to 82.0%. This increase aligns with the endothermic nature of CH₄ reforming with CO₂ at elevated temperatures (Awad *et al.*, 2024). For 10%Co/Al₂O₃ catalyst, the reduction in conversion over time for both CH₄ and CO₂ at 1023 K and 1073 K is minimal compared to the conversion at 973 K. Meanwhile, deactivation of the promoted catalyst was observed at higher temperatures. These observations indicate that the metallic Co (0) in the active phase is oxidized due to the abundant oxygen from the dissociative adsorption of CO₂ (Tran *et al.*, 2021).

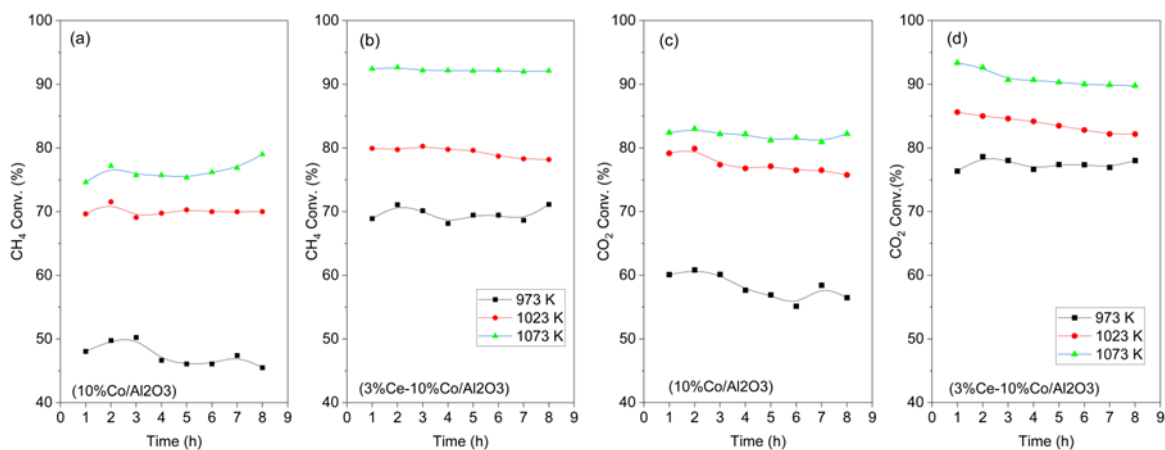


Figure 3: The CH₄ and CO₂ conversions as a function of reaction time using 10%Co/Al₂O₃ and 3%Ce-10%Co/Al₂O₃ catalysts

In the presence of the CeO₂ promoter, the conversion of CH₄ and CO₂ in the reforming reaction increases compared to the 10%Co/Al₂O₃ catalyst at all investigated temperature values. These results demonstrate the role of CeO₂ in enhancing catalytic activity in the reaction. The changes in the properties of 3%Ce-10%Co/Al₂O₃, such as the decrease in catalyst particle size and the ease of the reduction process, are believed to be factors influencing the catalyst's activity. Additionally, the basic properties of CeO₂ contribute to an increased adsorption of the acidic reactant CO₂, thereby promoting a faster reaction rate (Maziviero *et al.*, 2024).

The product yields for reactions conducted over the catalysts 3%Ce-10%Co/Al₂O₃ and 10%Co/Al₂O₃ at various temperatures are presented in Figures 4(a-c). For the 3%Ce-10%Co/Al₂O₃ catalyst, both CO and H₂ yields increased with rising temperature, reaching maximum values of 81.1% and 82.1%, respectively. The H₂/CO ratio ranged from 0.63 to 0.86 for the 10%Co/Al₂O₃ catalyst and from 0.85 to 1.00 for the 3%Ce-10%Co/Al₂O₃ catalyst. At all examined temperatures, this ratio remained consistently below 1, suggesting the occurrence of a reaction between CO₂ and H₂ that produces CO and H₂O, as represented in Equation 2.

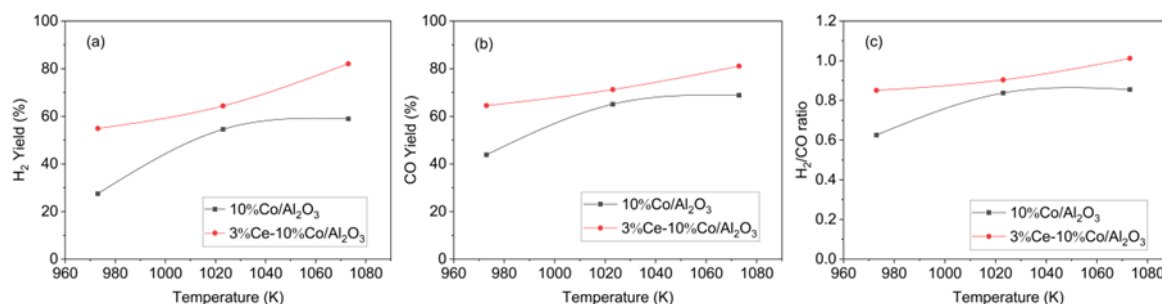


Figure 4: The H₂, CO yields and H₂/CO ratio as a function of reaction time using 10%Co/Al₂O₃ and 3%Ce-10%Co/Al₂O₃



Syngas with an H₂/CO ratio between 0.8 and 1.0 serves as an optimal feedstock for the synthesis of long-chain hydrocarbons through the Fischer-Tropsch process (Gray *et al.*, 2024). The HRTEM images of the catalyst samples before and after CH₄ reforming with CO₂ are shown in Figure 5a. In the fresh catalysts, Figures 5a(I-II), the gamma-phase Al₂O₃ is distinctly observed in both materials. However, cobalt oxide particles are more prominently observed in the 10%Co/Al₂O₃ catalyst compared to the 3%Ce-10%Co/Al₂O₃ catalyst. This observation is consistent with the significantly smaller particle size of cobalt oxide in the 3%Ce-10%Co/Al₂O₃ catalyst relative to the 10%Co/Al₂O₃ catalyst.

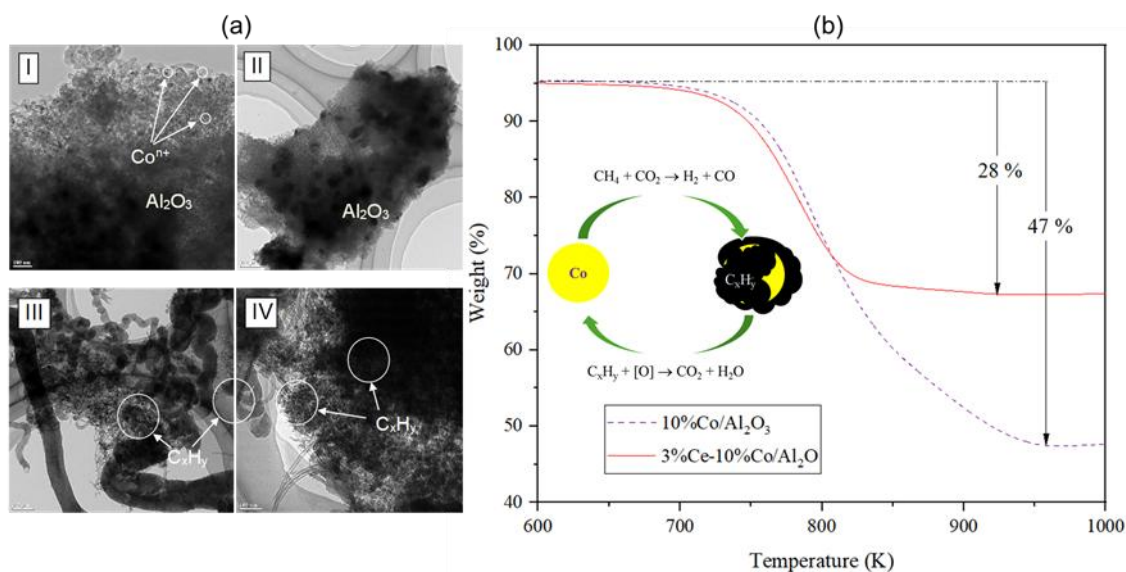


Figure 5: (a) TEM images of (I) 10%Co/Al₂O₃ fresh; (II) 3%Ce-10%Co/Al₂O₃ fresh; (III) spent 10%Co/Al₂O₃; (IV) spent 3%Ce-10%Co/Al₂O₃ and (b) TPO spectra of the catalysts after 8 hours reaction 1023 K

Figures 5a(III-IV) present the images of the 10%Co/Al₂O₃ and 3%Ce-10%Co/Al₂O₃ catalysts, respectively, after being used in reforming reaction at 1023 K. Carbon deposits (C_xH_y) accumulate around the catalyst particles, obstructing the active sites and limiting reactant access. Throughout the reaction, these carbon deposits are progressively eliminated via oxidation, allowing for the regeneration of the active sites. The TPO spectra reveal the carbon residue formed on the 10%Co/Al₂O₃ and 3%Ce-10%Co/Al₂O₃ catalysts after the reaction at 1023 K (Figure 5b). The carbon content on the 10%Co/Al₂O₃ catalyst was found to be 47%, whereas on the 3%Ce-10%Co/Al₂O₃ catalyst, it was 28%. This suggests that the carbon formation and release cycle on the surface of the 3%Ce-10%Co/Al₂O₃ catalyst occurs more rapidly, leading to lower carbon accumulation during the reaction. The reaction mechanism is illustrated in the embedded figure in the TPO spectra.

4. Conclusion

The Al₂O₃ support material, characterized by a mesoporous structure with uniform pore sizes, was synthesized and employed as support for the preparation of 3%Ce-10%Co/Al₂O₃ and 10%Co/Al₂O₃ catalysts. The structural integrity of the Al₂O₃ support is preserved, with minimal alterations during catalyst preparation. Notably, the introduction of 3%Ce into the catalyst results in beneficial changes to the physicochemical properties of the 3%Ce-10%Co/Al₂O₃ catalyst, enhancing its performance in the CH₄ reforming reaction with CO₂. Specifically, a decrease in particle size and a more efficient reduction of cobalt oxide to the active cobalt phase are observed. The catalytic performance for the CH₄ reforming reaction shows increased yields of CO and H₂, reaching 81.1% and 82.1%, respectively, at 1073 K. The H₂/CO ratio in the product ranges from 0.85 to 1.00, making it suitable for use as a feedstock in the Fischer-Tropsch synthesis of long-chain hydrocarbons. Additionally, the CeO₂ promoter in the 3%Ce-10%Co/Al₂O₃ catalyst is found to enhance CO₂ adsorption, promoting the oxidation of carbon deposits on the active sites and maintaining stable catalytic activity throughout the CH₄ reforming reaction with CO₂.

References

- Alhassan, M., Bin Bahari, B.M., Owgi, A. H. K. & Tran, T.V., 2024, non-noble metal catalysts for dry reforming of methane: Challenges, opportunities, and future directions, *EDP Sciences*, 516, 1-5.
- Ali, R., Mushtaq, S., Cheng, C. K., Wongsakulphasatch, S. & Al-Ali, K., 2024. Unveiling the potential of desert sand-derived mesoporous silica supported nickel-based catalysts for co-production of H₂ and carbon nanomaterials via methane cracking, *Fuel*, 377, 132758.
- Arora, N. K. & Mishra, I., 2021. COP26: more challenges than achievements, *Environmental Sustainability*, 4, 585 – 588.
- Awad, M. M., Hussain, I., Mustapha, U., Taialla, O.A., Alhassan, A.M., Kotob, E., Abdullahi, A.S., Ganiyu, S.A., Alhooshani, K., 2024, A critical review of recent advancements in catalytic dry reforming of methane: Physicochemical properties, current challenges, and informetric insights, *International Journal of Hydrogen Energy*, 76, 202 - 233.
- Gray, B., Johnson, O., B. Joseph, B. & Kuhn, J. N., 2024, High-Temperature Fe-Based Fischer-Tropsch Synthesis: Experimentally Validated Kinetic Models Implemented at Pellet and Reactor Scales, *Industrial & Engineering Chemistry Research*, 63(34), 15061 – 15072.
- Hernández, S., Farkhondehfal, M. A., Sastre, F., Makkee, M., Saracco, G. & Russo, N., 2017, Syngas production from electrochemical reduction of CO₂: current status and prospective implementation, *Green Chemistry*, 19(10), 2326–2346.
- Jiang, K., Ashworth, P., Zhang, S., Liang, X., Sun, Y. & Angus, D., 2020, China's carbon capture, utilization and storage (CCUS) policy: A critical review, *Renewable and Sustainable Energy Reviews*, 119, 109601 - 109616.
- Khivantsev, K., Jaegers, N. R., Kwak, J., Szanyi, J. & Kovarik, L., 2021, Precise Identification and Characterization of Catalytically Active Sites on the Surface of γ -Alumina, *Angewandte Chemie*, 133(32), 17663 - 17671.
- Liang, D., Wang, Y., Wang, Y., Chen, M., Xie, X., Li, C., Wang, J., Yuan, L., 2024, Dry reforming of methane for syngas production over noble metals modified M-Ni@ S-1 catalysts (M= Pt, Pd, Ru, Au), *International Journal of Hydrogen Energy*, 51, 1002 - 1015.
- Maziviero, F.V., Melo, D.M.A., Medeiros, R.L.B.A., Silva, J.C.A., Araújo, T.R., Oliveira, Â.A.S., Silva, Y.K.R.O., Melo, M.A.F., 2024, Influence of Mn, Mg, Ce and P promoters on Ni-X/Al₂O₃ catalysts for dry reforming of methane, *Journal of the Energy Institute*, 113, 101523.
- Nguyen, D. L. T., Tran, A.V., Vo, D.V.N., Nguyen, H.T., Rajamohan, N., Trinh, T.H., Nguyen, T.L., Le, Q.V., Nguyen, T.M., 2024. Methane dry reforming: A catalyst challenge awaits, *Journal of Industrial and Engineering Chemistry*, 140, 169 - 189.
- Tran, N.T., Le, Q.V., Cuong, N.V., Nguyen, T.D., Phuc, N.H.H., Phuong, P.T.T., Monir, M.U., Aziz, A.A., Truong, Q.D., Abidin, S.Z., Nanda, S., Vo, D.V.N., 2020, La-doped cobalt supported on mesoporous alumina catalysts for improved methane dry reforming and coke mitigation, *Journal of the Energy Institute*, 93(4), 1571 - 1580.
- Tran, N.T., Pham, T.L.M., Nguyen, T.D., Cuong, N.V., Siang, T.J., Phuong, P.T.T., Jalil, A.A., Truong, Q.D., Abidin, S.Z., Hagos, F.Y., Nanda, S., Vo, D.V.N., 2021, Improvements in hydrogen production from methane dry reforming on filament-shaped mesoporous alumina-supported cobalt nanocatalyst, *International Journal of Hydrogen Energy*, 46 (48), 24781 - 24790.